Electrically Induced Raman Emission from Planar Spin Oscillator

A. Nogaret*

Department of Physics, University of Bath, Claverton Down, Bath, BA2 7AY, United Kingdom

(Received 22 July 2004; published 14 April 2005)

We predict that two-dimensional electrons confined by a magnetic field gradient resonantly transfer energy to the electromagnetic field by a process of inverse electron spin resonance that is realized when the frequency of an open orbit equals the Larmor frequency. The calculated emission spectra show multiple peaks modulated by strong optical nonlinearities whose frequencies may be tuned by the magnetic field gradient and the electron concentration.

DOI: 10.1103/PhysRevLett.94.147207 PACS numbers: 85.75.−d, 73.23.−b, 76.20.+q

Optical pumping with anisotropic light has long been studied in atoms [1], impurities [2], and semiconductors [3–5] to induce magnetic polarization or inversely to obtain circularly polarized light from the recombination of a spin polarized current [6]. Light emission from pure magnetodipole coupling has comparatively been difficult to demonstrate in the solid state despite arising naturally elsewhere [7,8]. One way for an electron spin to gain energy is by traversing a region of spatially inhomogeneous magnetic field. Because of advances in microfabrication, such magnetic modulations can now be applied to low-dimensional electron systems [9–12]. Hybrid confinement by electrostatic potentials and magnetic field gradients introduce an artificial means of coupling the spin and orbital motion to induce spin resonant effects impossible to obtain through conventional spin-orbit coupling [13,14].

In this Letter, I demonstrate the generation of electromagnetic (EM) radiation through the process of inverse spin resonance. This is realized when a spin $1/2$ charged particle is confined to a plane and subjected to both an in-plane homogeneous magnetic field and a perpendicular magnetic field gradient. Particles drifting in open orbits, near a line of zero transverse magnetic field, have an oscillatory motion that subjects the spin magnetic moment to a periodic magnetic field. In the steady state, the magnetic dipole oscillator converts electrical energy into light. The EM emission spectrum is found to peak near the cutoff frequency of the open orbits. The amplitude and helicity of light are, respectively, controlled by the current intensity and the spin polarization of the injected current. The emission lines correspond to NMR absorption frequencies which is of interest to quantum computation [15,16].

Without loss of generality, we consider the system shown in Fig. 1. A hard ferromagnetic wire is placed at the surface of a semiconductor quantum well structure containing a two-dimensional electron system (2DES) that for illustration purposes we shall assume to be InAs. The wire magnetization, set parallel to the z axis, induces a stray magnetic field that has vector components B_x and B_z at the level of the 2DES. At a depth comparable to the wire thickness [9–11], B_z is approximately constant across the wire and B_x is of the form $B_x = bz$. Electrons near the center of the wire keep oscillating between the $B_x > 0$ and $B_x < 0$ regions as they drift in open "snake" orbits guided by the $B_x = 0$ line [9,12,17]—see Fig. 1(b). In such orbits, the electron spin views an ac magnetic field oscillating at the snake frequency and whose amplitude grows with the lateral extent of the snake oscillations. The electron spin concurrently precesses around B_z at the Larmor frequency $\omega_0 = -\gamma B_z$ where γ is the spin gyromagnetic ratio. The cross dc and ac magnetic fields set the background for electron spin resonance that is realized when the Larmor frequency equals the snake orbit frequency $\omega = \omega_0$. Here, however, the work done by the ac magnetic field on the spin is transferred to the EM field, a situation reverse of conventional magnetic resonance where the ac magnetic field is supplied by the modes of an EM cavity. Under equal injection of spin up and spin down currents, photon emission is linearly polarized along B_x. The role of the ferromagnetic contacts, shown in Fig. 1(b), is to inject a net

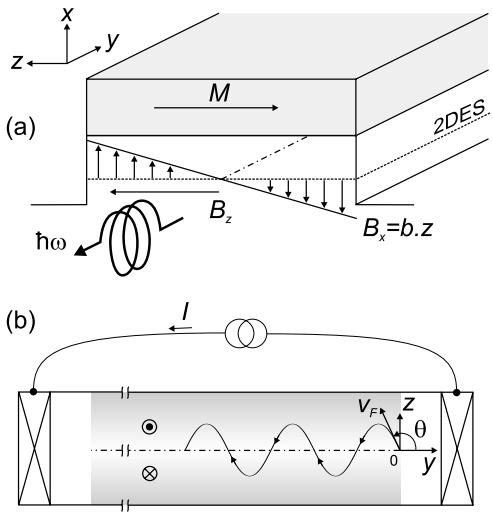

FIG. 1. (a) Magnetic waveguide cross section. (b) A spin polarized current is injected into the 2DES through ferromagnetic contacts magnetized along z. The 2DES section located below the ferromagnetic wire is subjected to both a magnetic field gradient from the stray vector component B_x (amplitude ≡ level of gray) that channels electrons in snake states and a constant B_z that sets the spin Larmor frequency.

magnetic moment into the waveguide so that the output wave acquires partial circular polarization. The injection of a spin up (down) current generates σ^+ (σ^-) photons, respectively, to comply with the conservation of angular momentum. As electrons progress inside the waveguide, nonlinearity tends to equalize spin up and spin down populations. Nonlinearity manifests here to a hitherto unprecedented degree due to the simultaneous occurrence of (i) a rich spectrum of harmonics in $B_x(t)$ induced by the anharmonicity of snake oscillations, (ii) saturation effects and multiple photon emission due to B_x being of the same order of magnitude as B_z. The following derivation contains two parts. The frequency spectrum of snake states, the ac magnetic field $B_x(t)$, and the spin injection rate into a snake orbit are first obtained. We then describe the spin dynamics in the waveguide and compute its EM emission spectrum.

An appropriate description of electron dynamics in magnetic gradients is accessible at the semiclassical level [18,19]. The equation of motion $m^*\dot{\mathbf{v}} = -e\mathbf{v} \times \mathbf{B}$ applied to an electron with velocity $\mathbf{v}$, charge $-e$, and effective mass m^* can be written in the form

$$\tau_b \dot{Y} = \cos(\theta)/2 - Z^2, \tag{1}$$

$$(\tau_b \dot{Z})^2 = [\cos^2(\theta/2) - Z^2][Z^2 + \sin^2(\theta/2)], \tag{2}$$

where $Y \equiv y/l_b$ and $Z \equiv z/l_b$ are the dimensionless coordinates and θ is the angle at which a snake orbit crosses the $B_x = 0$ line. This orbit oscillates between $Z = \pm\cos(\theta/2)$ as obtained by setting $\dot{Z} = 0$ in Eq. (2). The length scale $l_b \equiv 2\sqrt{\hbar k_F/(eb)}$ thus characterizes the amplitude of the largest oscillations that occur at $\theta = 0$. Here $k_F = \sqrt{2\pi n_s}$ and n_s is the 2DES electron density. Magnetic gradients also introduce the time scale $\tau_b \equiv m^*/\sqrt{\hbar k_F eb}$ that can be understood by considering an orbit which touches the $Z = 1$ line. Such an orbit never completes a full turn because it approaches the $Z = 0$ line asymptotically such that $Z \propto \exp(-t/\tau_b)$. An InAs quantum well with $n_s = 1 \times 10^{15}$ m^{-2} and subjected to a magnetic gradient $b = 2 \times 10^6$ T/m would have $l_b = 323$ nm and $\tau_b = 0.41$ ps.

After integrating Eq. (2), we find the time dependence of Z to be $t = \tau_b F(\chi, \theta)$ where F is the elliptic integral [20]

$$F(\chi, \theta) = \int_0^{\chi} \frac{d\alpha}{\sqrt{1 - \cos^2(\theta/2)\sin^2(\alpha)}} \tag{3}$$

and $\chi = \arcsin\sqrt{Z^2/\{\cos^2(\theta/2)[Z^2 + \sin^2(\theta/2)]\}}$. At a quarter of the period, $Z = \cos(\theta/2)$ so that the snake orbit period is given by $T \equiv 4\tau_b F(\pi/2, \theta)$. Since Eq. (2) describes an anharmonic oscillator, we seek $Z(t)$ as a Fourier expansion of the fundamental frequency $\omega = 2\pi/T$. The antisymmetry of the magnetic field $B_x(z) = -B_x(-z)$ and its translational invariance along y simplify the integration of the Fourier coefficients and after integration by parts, one obtains

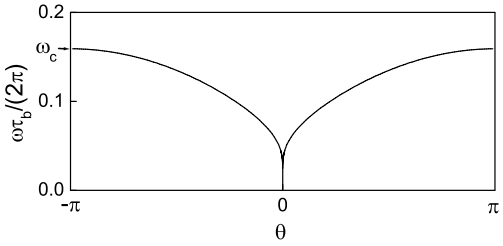

FIG. 2. Snake state frequency as a function of initial angle θ.

$$Z(t) = \sum_{k=0}^{\infty} b_{2k+1} \sin[(2k+1)\omega t],$$

$$b_{2k+1} = \frac{4}{(2k+1)\pi} \int_0^{\cos(\theta/2)} dZ \cos\left[\frac{(2k+1)\pi}{2} \frac{F(\chi, \theta)}{F(\pi/2, \theta)}\right]. \tag{4}$$

Hence the ac magnetic field experienced by the electron spin in snake orbit θ is $B_x(t) = bl_b Z(t)$.

Figure 2 shows the frequency of snake oscillations as a function of θ. As $\theta \to 0$, snake orbits tend to approach the $Z = 0$ line asymptotically and therefore have infinite period. As $\theta \to \pi$, the oscillator frequency presents a *cutoff* at $\omega_c \approx 0.16(2\pi)/\tau_b$. When $\theta \sim \pi$, snake oscillations are quasisinusoidal and become more complex as θ approaches 0.

The ferromagnetic electrodes attached to the magnetic waveguide in Fig. 1(b) inject spins at a rate $n_0 \equiv \beta I/e$ where $\beta \equiv (I_\uparrow - I_\downarrow)/I$ is the spin polarization [21]. As these enter the magnetic gradient at $Y = 0$, they distribute among accessible snake states according to a function $n(\theta)$ that we now calculate. A snake orbit is accessible if the height of the incoming spin (Z_0) is within a certain range $\Delta Z = Z_{\max} - Z_{\min}$. $Z_{\max} \equiv \cos(\theta/2)$ and corresponds to injection at the snake orbit maximum—set $\dot{Z} = 0$ in Eq. (2). $Z_{\min} \equiv \sqrt{\cos(\theta)/2}$ corresponds to injection into an orbit with vanishing longitudinal velocity—set $\dot{Y} = 0$ in Eq. (1). ΔZ is plotted as the blank region in Fig. 3(a). The sum of all current contributions in this range gives $n(\theta)$. Each snake orbit carries a current proportional to $\langle v_y \rangle_\tau = \tau^{-1} \int_0^\infty dt v_y \exp(-t/\tau)$ where τ is the momentum scattering time. Using Eqs. (1) and (4) one finds

$$\frac{\langle v_y \rangle_\tau}{v_F} = \cos(\theta) - \sum_{k=0}^{\infty} \sum_{k'=0}^{\infty} b_{2k+1} b_{2k'+1} \left[\frac{\cos[2(k-k')\omega t_0] + [2(k-k')\omega\tau]\sin[2(k-k')\omega t_0]}{1 + [2(k-k')\omega\tau]^2} \right.$$
$$\left. - \frac{\cos[2(k+k'+1)\omega t_0] + [2(k+k'+1)\omega\tau]\sin[2(k+k'+1)\omega t_0]}{1 + [2(k+k'+1)\omega\tau]^2} \right], \tag{5}$$

where $t_0 = \tau_b F[\chi(Z_0), \theta]$ is the time taken by the electron trajectory to reach height Z_0. The full line in Fig. 3(b) shows the

average snake velocity in the diffusive regime corresponding to $\tau = 1$ ps. Interestingly, this velocity reverses at a critical angle, $\theta_c^{1\mathrm{ps}} \approx 60°$. This occurs because of the formation of the two types of orbits shown in the inset to Fig. 3(b). In the special case of the ideal 2DES ($\tau \to \infty$), Eq. (5) reduces to $\langle v_y \rangle / v_F = \cos(\theta) - \sum_{k=0}^{\infty} b_{2k+1}^2$ and one recovers the critical angle $\theta_c^{\infty} \approx 49°$ obtained by Evers *et al.* [19]— see dotted line plots. Since snake states in the ranges $\Theta_+ = [0 - \theta_c]$ and $\Theta_- = [\theta_c - \pi]$ carry opposite currents, $n(\theta)$ writes as

$$n(\theta) = n_0 \langle\langle v_y \rangle_\tau \rangle_{\Delta Z} / \langle\langle\langle v_y \rangle_\tau \rangle_{\Delta Z} \rangle_{\Theta_\pm}. \tag{6}$$

Equation (6) is plotted in Fig. 3(c). The injection rate is higher into fast traveling orbits and one verifies that $n(\theta)$ averages to n_0 over the Θ_+ and Θ_- intervals.

The time evolution of the magnetic moment $\mathbf{m}(t)$ carried by a statistical ensemble of spins inside the waveguide must satisfy

$$\dot{\mathbf{m}} = n(\theta)\mu^* \mathbf{e_z} + \gamma \mathbf{m} \times \mathbf{B(t)} - \mathbf{m}/\tau_s. \tag{7}$$

The first term to the right describes the rate of change of $\mathbf{m}$ due to the injection of magnetic moments $\mu^* \equiv g\mu_B/2$ where g is the Landé factor and μ_B the Bohr magneton. The middle term reduces to the classical rate of change of $\mathbf{m}$ induced by the magnetic torque acting on $\mathbf{m}$ [22]. Finally the magnetic moment may decay as a result of electrons exiting the waveguide, scattering out of a snake orbit or as a result of spin relaxation. The momentum scattering time being shorter than both the electron dwell time in the waveguide and the spin lifetime in semiconductors [3,5], we take $\tau_s \approx \tau$. After making the standard change of variable $m_\pm = m_x \pm i m_y$, Eq. (7) becomes

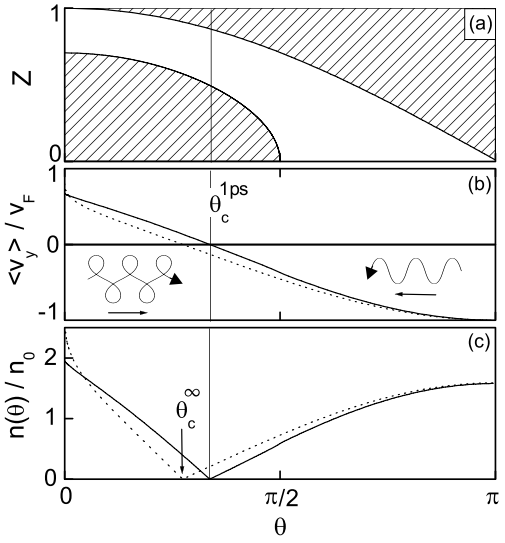

FIG. 3. (a) The interval between the two hatched areas corresponds to the range of θ values accessible to a snake orbit crossing a point of height Z. (b) Average snake velocity and (c) spin injection rate into snake orbit θ when $\tau \to \infty$ (dotted line) and $\tau = 1$ ps (full line). The inset trajectories in (b) drift in opposite directions when $\theta < \theta_c$ and $\theta > \theta_c$.

$$\begin{cases} \dot{m}_z = n\mu^* + i\omega_1(m_- - m_+)Z(t)/2 - m_z/\tau_s \\ \dot{m}_\pm = \pm i[\omega_0 m_\pm - \omega_1 m_z Z(t)] - m_\pm/\tau_s, \end{cases} \tag{8}$$

where $\omega_0 = -\gamma B_z$, $\omega_1 = -\gamma b l_b$ and $Z(t)$ is given by Eq. (4). Equation (8) is a nonlinear system that we solve using Bloembergen's ansatz [22,23]. Namely, one seeks solutions in the form of a polynomial expansion in powers of the ac magnetic field: $m_z = \sum_{q=0}^{\infty} \omega_1^{q\,(q)} m_z$ and $m_\pm = \sum_{q=0}^{\infty} \omega_1^{q\,(q)} m_\pm$. The time dependence of coefficients ${}^{(q)}m_z$ and ${}^{(q)}m_\pm$ is in turn expanded as a Fourier series: ${}^{(q)}m_z = \sum_{p=-\infty}^{+\infty} {}_p^{(q)} m_z \exp(ip\omega t)$ and ${}^{(q)}m_\pm = \sum_{p=-\infty}^{+\infty} {}_p^{(q)} m_\pm \times \exp(ip\omega t)$. Substitution into Eq. (8) gives

$$\begin{aligned} {}_p^{(q)}m_z &= \sum_{k=0}^{\infty} \frac{b_{2k+1}}{4[ip\omega + \Gamma_s]} \Big[{}_{p-(2k+1)}^{(q-1)}m_- - {}_{p+(2k+1)}^{(q-1)}m_- \\ &\quad - {}_{p-(2k+1)}^{(q-1)}m_+ + {}_{p+(2k+1)}^{(q-1)}m_+ \Big] \\ {}_p^{(q)}m_\pm &= \sum_{k=0}^{\infty} \frac{\mp b_{2k+1}}{2[ip\omega \mp i\omega_0 + \Gamma_s]} \\ &\quad \times \Big[{}_{p-(2k+1)}^{(q-1)}m_z - {}_{p+(2k+1)}^{(q-1)}m_z \Big] \end{aligned} \tag{9}$$

for $q > 0$ where $\Gamma_s = 1/\tau_s$. At order 0 ($q = 0$), ${}_0^{(0)}m_z = n\mu^*\tau_s$, and ${}_p^{(0)}m_z = 0$ for $p \neq 0$ while ${}_p^{(0)}m_\pm = 0$ for all p. The magnetic moment at order 1 is obtained by substituting the terms of order 0 into Eq. (9). Subsequent corrections to higher order are calculated recursively using Eq. (9). The instantaneous work done by the field on the magnetic moment follows as $-\dot{\mathbf{m}} \cdot \mathbf{B}$. This is averaged over the snake orbit period to find the average absorbed power $[p(\theta)]$. In the steady state this power is radiated because spin lattice relaxation is completely negligible over the precession period. We calculate $p(\theta)$ to the third order and find terms of the form $p = {}^{(1)}p + {}^{(3)}p_0 + {}^{(3)}p_{3\omega} + {}^{(3)}p_\omega$. The leading term is:

$${}^{(1)}p = \frac{n\hbar\omega}{8} \sum_{k=0}^{\infty} (2k+1) b_{2k+1}^2 \Big[\frac{\omega_1^2}{[\omega_0 - (2k+1)\omega]^2 + \Gamma_s^2} - \frac{\omega_1^2}{[\omega_0 + (2k+1)\omega]^2 + \Gamma_s^2} \Big] \tag{10}$$

Equation (10) shows that the emission spectrum consists of two series of peaks at $\omega = \pm\omega_0/(2k+1)$. The positive series corresponds to σ^+ photons emitted by spin up injection ($n > 0$) whereas the negative series accounts for σ^- photon emission from down spins ($n < 0$). The main peak at $k = 0$ occurs when the Larmor frequency is resonant with the fundamental frequency of the snake oscillator. The emission lines $k = 1, 2 \ldots$ are the resonances with the harmonics of the ac magnetic field. Their amplitude is usually comparable to the main resonance because the lower frequencies in Fig. 2 are produced by snake orbits near $\theta \sim 0$ that display the greatest anharmonicity. Figure 4 plots Eq. (10) (dotted lines) for three values of the Larmor frequency around ω_c. As the Larmor frequency

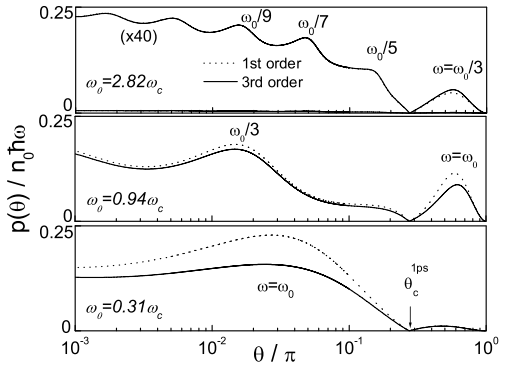

FIG. 4. Number of photons emitted by snake orbit θ per spin injected in the waveguide for three Larmor frequencies ω_0. ($\tau =$ 1 ps, $b = 2 \times 10^6$ T/m, $m^* = 0.023m_0$, $g = -15$).

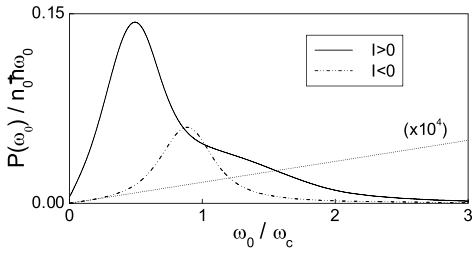

FIG. 5. Number of photons emitted per spin injected in the waveguide when $I > 0$ (full line) and $I < 0$ (dash-dotted line). The power radiated by the oscillating snake current is shown as the straight dotted line ($\beta = 10\%, I = 1\ \mu$A).

increases from $0.31\omega_c$ to $2.82\omega_c$, the $k = 0$ resonance shifts to higher values of θ. It then disappears when it is no longer possible to find a snake frequency matching the Larmor frequency. In the top panel, the only resonances left are those involving the higher harmonics of the ac field that satisfy $\omega_0/(2k + 1) < \omega_c$.

The full lines in Fig. 4 plot $p(\theta)$ including third order corrections. The ${}^{(3)}p_0$ term has the overall effect of *reducing* the amplitude of emission lines. This is because transitions between spin up and spin down states tend to reduce the imbalance between the two spin populations. The ${}^{(3)}p_{3\omega}$ and ${}^{(3)}p_{\omega}$ terms account for 3 photon emission processes via virtual quantum states. For example, the $\omega_0/3$ peak in the top panel of Fig. 4 is *enhanced* by the cascade emission of three photons with energy $\hbar\omega_0/3$.

Figure 4 shows the power emitted by individual snake states. More relevant to experiments is the integrated power, $P(\omega_0) = \langle p(\theta)\rangle_{\Theta_\pm}$, emitted by the bundle of snake states. This is plotted in Fig. 5 as a function of the Larmor frequency. For $I > 0$, $P(\omega_0)$ peaks at $0.5\omega_c$ when snake orbits near $\theta \approx 23°$ resonate at their fundamental frequency— see Fig. 2. The shoulder at $1.5\omega_c$ corresponds to the resonance of their first harmonic. For $I < 0$, $P(\omega_0)$ peaks at $0.9\omega_c$ when snake orbits near $\theta \approx 105°$ resonate. This finding has significant practical interest for EM sources since ω_c only depends on b, n_s, and m^*. The range of values taken by these parameters indicates that emission lines are tunable in the 0–500 GHz bandwidth. These lines are robust against temperature since $\tau = 1$ ps is the mobility scattering time at 230 K in InAs. This anisotropic light source is well suited to the manipulation of nuclear spins in quantum computation. We anticipate that magnetic waveguides could be biassed with current pulses of calibrated amplitude and duration to tip nuclear spins underneath the 2DES.

For the sake of completeness, we compare the power radiated by the resonating electron spins with the power radiated by the ac snake current which is akin to a small antenna of length $2l_b$ [24]. The latter is shown as the straight dotted line in Fig. 5 and is seen to be over 4 orders of magnitude smaller.

In summary, we have demonstrated Raman emission and high harmonic generation from an electrically driven spin resonator. Spatially varying electric and magnetic fields may be combined to provide artificial spin-orbit coupling.

It is a pleasure to acknowledge discussions with Professor S. J. Bending and Professor J. J. Davies.

*Electronic address: A.R.Nogaret@bath.ac.uk

[1] Hanle.W, Z. Phys. **30**, 93 (1924).
[2] R. Geschwind, S. Collins, and A. Schawlow, Phys. Rev. Lett. **3**, 545 (1959).
[3] S. Ganichev *et al.*, Nature (London) **417**, 153 (2002).
[4] M. Poggio *et al.*, Phys. Rev. Lett. **91**, 207602 (2003).
[5] J. Kikkawa and D. Awschalom, Science **287**, 473 (2000).
[6] R. Fiederling *et al.*, Nature (London) **402**, 787 (1999).
[7] B. Draine and A. Lazarian, Astrophys. J. **512**, 740 (1999).
[8] B. Draine and A. Lazarian, Astrophys. J. **494**, L19 (1998).
[9] A. Nogaret, S. Bending, and M. Henini, Phys. Rev. Lett. **84**, 2231 (2000).
[10] M. Hara *et al.*, Phys. Rev. B **69**, 153304 (2004).
[11] V. Kubrak *et al.*, Appl. Phys. Lett. **74**, 2507 (1999).
[12] P. D. Ye *et al.*, Phys. Rev. Lett. **74**, 3013 (1995).
[13] M. D'yakonov and V. Perel, Sov. Phys. JETP **33**, 1053 (1971).
[14] Y. Yafet, Solid State Phys. **14**, 1 (1963).
[15] D. DiVincenzo, Science **270**, 255 (1995).
[16] N. Gershenfeld and I. Chuang, Science **275**, 350 (1997).
[17] J. Reijniers and F. Peeters, Phys. Rev. B **63**, 165317 (2001).
[18] D. Lee, J. Chalker, and D. Ko, Phys. Rev. B **50**, 5272 (1994).
[19] F. Evers *et al.*, Phys. Rev. B **60**, 8951 (1999).
[20] I. Gradshteyn and I. Ryzhik, *Tables of Integrals Series and Products* (Academic, New York, 1965).
[21] Parallel conduction through edge states and cycloid states is ignored here as these states are nonradiative [17].
[22] C. Cohen-Tannoudji, B. Diu, and F. Laloë, *Quantum Mechanics* (John Wiley & Sons, New York, 1986), 3rd ed.
[23] N. Bloembergen, *Nonlinear Optics* (World Scientific, London, 1992), 4th ed.
[24] J. Jackson, *Classical Electrodynamics* (John Wiley & Sons, New York, 1999), 3rd ed.